ELSEVIER

Polymer 43 (2002) 7315–7323

polymer

www.elsevier.com/locate/polymer

Crystal structure of poly(pentamethylene 2,6-naphthalate)

Young Gyu Jeong[a], Won Ho Jo[a,*], Sang Cheol Lee[b,*]

[a]*Hyperstructured Organic Materials Research Center and School of Materials Science and Engineering, Seoul National University, Seoul 151-742, South Korea*

[b]*School of Material and System Engineering, Kumoh National University of Technology, Kumi 730-701, South Korea*

Received 1 July 2002; received in revised form 5 September 2002; accepted 13 September 2002

Abstract

The crystal structure of poly(pentamethylene 2,6-naphthalate) (PPN) was determined by using X-ray diffraction and molecular modeling. The unit cell of PPN was found to be triclinic ($P\bar{1}$ space group) with dimensions of $a = 0.457$ nm, $b = 0.635$ nm, $c = 2.916$ nm, $\alpha = 121.6°$, $\beta = 90.4°$, $\gamma = 87.6°$, and the calculated crystal density was 1.311 g cm^{-3}. The unit cell contains one polymer chain with two repeating units. In the unit cell, the PPN backbone takes *gauche*/*gauche* conformation in the middle part of each pentamethylene unit, and two naphthalene rings are in face-to-face arrangement.

Keywords: Poly(pentamethylene 2,6-naphthalate); Crystal structure; X-ray diffraction

1. Introduction

Aromatic polyesters derived from diols and diacids have attracted much attention for a long time due to their good thermal and mechanical properties. Among these polyesters, the family of poly(*m*-methylene 2,6-naphthalate) (P*m*N, where *m* is the number of methylene unit) with the chemical structure as shown in Fig. 1 was first reported in 1969 [1]. Since 2,6-naphthalene dicarboxylic acid has recently been produced in large-scale quantity, polyesters based on this monomer have shown high potential as an engineering plastic.

The most well-known polymer of this family is poly(ethylene 2,6-naphthalate) (PEN, $m = 2$), whose crystal structure, thermal properties, and mechanical properties have been intensively studied. It has been reported that PEN has two crystal structures, i.e. α-form and β-form, depending upon the crystallization temperature [2–4]. The α-form has a triclinic unit cell with a fully extended chain, and the β-form has also a triclinic unit cell but contains four chains with non-*trans* conformation. It has also been reported that poly(butylene 2,6-naphthalate) (PBN, $m = 4$) exhibits two crystal structures, i.e. A-form and B-form, depending upon the crystallization temperature and the applied stress [5,6]. The major difference between these two crystal structures of PBN is seen in the fiber period (*c*-axis), due to the difference in the molecular conformation of the butylene units as in the case of poly(butylene terephthalate) [7–9], i.e. the main chain in the B-form crystal is more extended than that in the A-form crystal. Recently, we have identified the crystal structures of poly(trimethylene 2,6-naphthalate) (PTN, $m = 3$) and poly(hexamethylene 2,6-naphthalate) (PHN, $m = 6$) [10–12]. It was found that both PTN and PHN have also two crystal structures, α-form and β-form, depending upon the crystallization temperature. The trimethylene units of PTN backbone in both crystal structures take *gauche*/*gauche* conformation [10], whereas the hexamethylene units in both crystal structures of PHN take nearly all-*trans* conformation [11,12]. In summary, PEN, PTN, PBN and PHN show polymorphism induced by temperature and/or stress. Among the P*m*N family, the crystal structure, thermal and physical properties of poly(pentamethylene 2,6-naphthalate) (PPN, $m = 5$) have not been investigated yet.

In this study, as the first step of systematic studies on PPN, its crystal structure is identified using X-ray diffraction and molecular modeling. In molecular modeling, molecular mechanics calculation is used.

* Corresponding authors. Tel.: +82-2-880-7192; fax: +82-2-885-1748.
E-mail addresses: whjpoly@plaza.snu.ac.kr (W.H. Jo), leesc@knut.kumoh.ac.kr (S.C. Lee).

0032-3861/02/$ - see front matter
PII: S0032-3861(02)00661-4

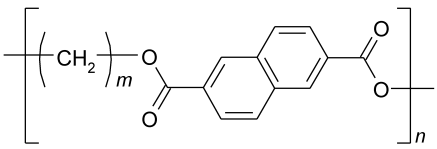

Fig. 1. Chemical structure of poly(*m*-methylene 2,6-naphthalate).

2. Experimental

2.1. Synthesis and characterization of PPN

PPN used in this study was synthesized by two step melt-condensation of 1,5-pentanediol with dimethyl-2,6-naphthalate using tetraisopropyl orthotitanate as a catalyst. The intrinsic viscosity of PPN measured in a mixed solvent of phenol/1,1,2,2-tetrachloroethane (6/4, v/v) at 35 °C with an Ubbelohde capillary viscometer was 0.67 dl/g, indicating that the synthesized sample has relatively high molecular weight enough to form in monofilament or in film. When the glass transition and melting temperatures of PPN were measured using a Perkin–Elmer DSC-7 equipped with intercooler system, the values were 40 and 115 °C, respectively. The density was measured using a Mettler AT200 balance (Mettler-Toledo Inc.). The density (ρ_1) of sample was estimated using the equation of $\rho_1 = A\rho_0/(A - B)$, where A and B denote the weight of sample measured in air and in distilled water, respectively, and ρ_0 is the density of distilled water.

2.2. Sample preparation

The monofilament of 1.0 mm in diameter was prepared by using a capillary rheometer (D8052B, Kayeness Inc.) and drawn to the strain between 2 and 6 at 50 °C on an universal tensile machine (LR 10K, Lloyd Inc.) with the cross-head speed of 0.1–1 cm min^{-1}. Subsequently, the monofilaments drawn uniaxially were annealed at 100 °C under constant strain or constant stress condition. The fine powder of PHN for obtaining X-ray powder diffractograms was prepared by the solution/precipitation method and annealed at various crystallization temperatures. The amorphous and crystalline samples were prepared by heating to the temperature 30 °C higher than the melting temperature, holding for 3 min in order to completely melt crystals, and rapidly transferring into cooling water or into another hot plate set at the predetermined crystallization temperature, respectively.

2.3. X-ray diffraction measurement

The X-ray fiber diagrams of monofilaments drawn uniaxially and annealed were recorded on a DIP2030 X-ray system (MAC Science Co.) with the flat imaging plate as a detector and Cu Kα radiation as an X-ray source (40 kV and 80 mA). The monofilament was arranged in the draw direction perpendicular to X-ray beam, and the sample-to-detector distance was about 80 mm.

Indexing of the reflection spots and unit cell parameters were determined by a trial and error method. The unit cell parameters were refined by minimizing the sum of square of the difference between the d-spacing (d_{obs}) evaluated from the location of diffraction spots and that (d_{cal}) calculated from the unit cell. The reliability parameter of indexing is expressed by the following equation:

$$R_{\text{X-ray}} = \left[\frac{\sum (d_{obs} - d_{cal})^2}{\sum d_{obs}} \right]^{1/2} \times 100\ (\%)$$

Two-dimensional intensity distribution of X-ray fiber diagram was read out from the X-ray diffraction data on the image plate and then stored as pixel data (3000 × 3000 pixels, 100 μm a pixel) of Cartesian coordinates. The intensity of a diffraction spot is expressed as

$$I = ALp|F_{obs}|^2 \exp(-2B \sin^2\theta/\lambda^2)$$

where A, L, p, $|F_{obs}|$, and B are the X-ray absorption coefficient of the sample, the Lorentz factor, the polarization factor, the observed structure factor, and the isotropic temperature factor, respectively. The observed structure factors ($|F_{obs}|$) were evaluated from intensity measurement after removing the background intensity and correcting the Lorentz and polarization factors. The absorption effect was not taken into account in this study.

The X-ray powder diffractograms of annealed PHN powders were obtained using a M18XHF diffractometer (MAC Science Co., Cu Kα radiation, 50 kV and 100 mA) at a scanning rate of 2° min^{-1}. The diffractometer was equipped with a $2\theta/\theta$ goniometer, a divergence slit (1.0°), a scattering slit (1.0°), and a receiving slit (0.30 mm). The X-ray measurements were performed at room temperature. The sample-to-detector distance or d-spacing was calibrated using Si powder ($2\theta = 28.44°$) as a standard for all X-ray diffraction measurements.

2.4. Molecular modeling technique

The crystal structure modeling with the aid of molecular mechanics calculation was carried out using commercially available software Cerius^2 (version 4.0, Molecular Simulation Inc.) on a Silicon Graphics Indigo II workstation. The total potential energy of a molecular chain consists of the contributions from the intramolecular and intermolecular interactions. The intramolecular interactions consist of the bond stretching, angle bending, torsional, and inversion terms. The intermolecular interactions include van der Waals and Coulomb terms. The COMPASS force field [13] was used to calculate the potential energy of crystal structure, and the Ewald summation method was used in the energy-minimizing calculation [14–16]. Standard bond lengths and angles for polyesters were adopted to build the repeating unit, and then the repeating unit length was adjusted to match it with the experimental c-axis. The chain was then translated and rotated within the unit cell in order

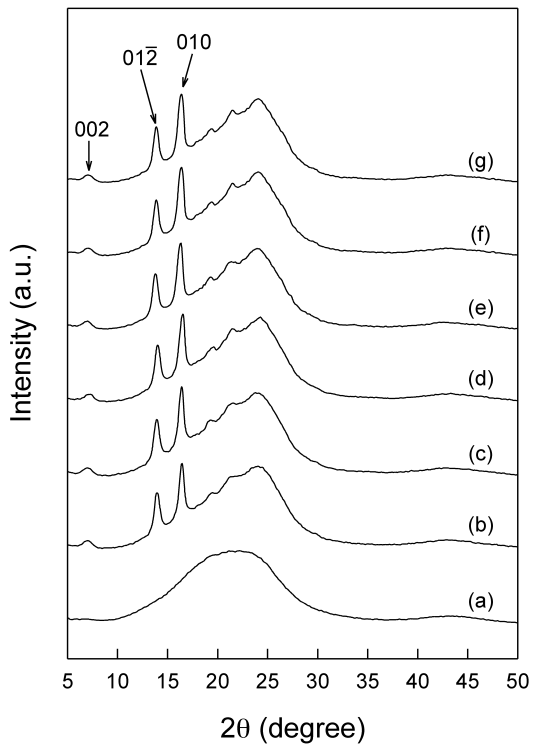

Fig. 2. X-ray diffractograms of PPN powders crystallized at various temperatures: (a) amorphous; (b) 60 °C; (c) 70 °C; (d) 80 °C; (e) 90 °C; (f) 100 °C; (g) 110 °C.

to minimize the packing interaction. During the energy minimization, the unit cell parameters were kept constant. The structure factors ($|F_{cal}|$) were calculated using the atomic coordinates corresponding to the energy-minimized conformation of the chain in the unit cell. The scale factor and overall isotropic temperature factor were refined to minimize the difference between $|F_{cal}|$ and $|F_{obs}|$. The

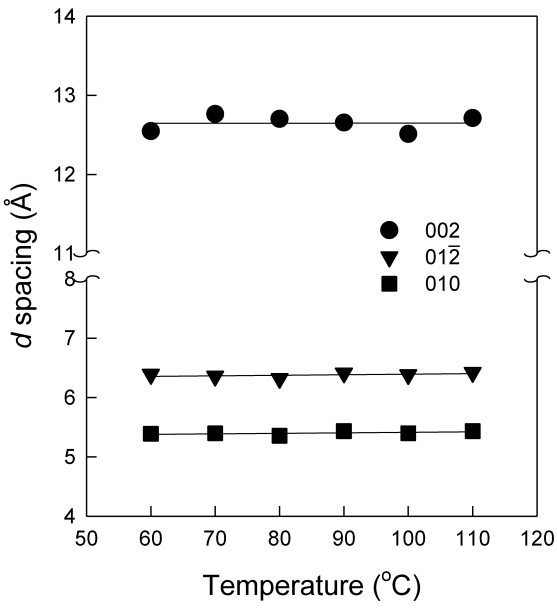

Fig. 3. Change of *d*-spacings with the crystallization temperature.

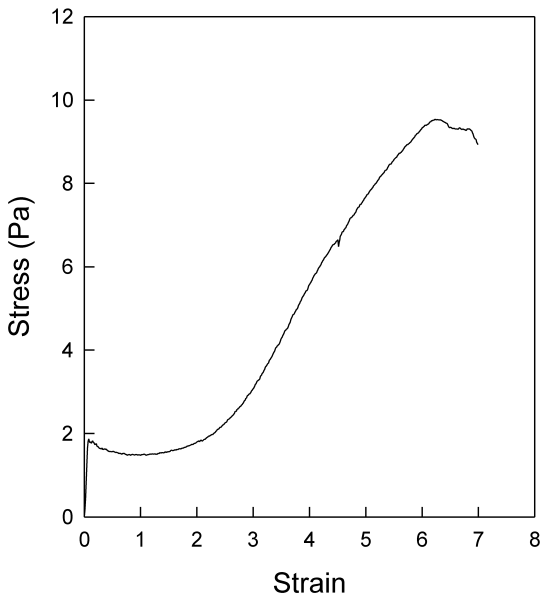

Fig. 4. Stress–strain curve of PPN monofilament measured at 50 °C under a drawing speed of 1 cm min^{-1}.

reasonability of the final crystal structure was evaluated by using the following reliability factor (R):

$$R = \frac{\sum||F_{obs}| - |F_{cal}||}{\sum|F_{obs}|} \times 100\ (\%)$$

3. Results and discussion

3.1. The effect of temperature and stress on the X-ray diffraction pattern of PPN

When the PPN sample is annealed at various temperatures for several days, the X-ray powder diffraction patterns show that several diffraction peaks are clearly observed and remain unchanged irrespective of the crystallization temperature, as shown in Fig. 2. When the *d*-spacings of three different reflections are plotted against the crystallization temperature, it reveals that the *d*-spacings remain nearly unchanged, as shown in Fig. 3. Therefore, it is concluded that the crystal transformation induced by temperature does not occur in PPN.

To investigate the effect of stress on the crystal structure, PPN monofilaments were uniaxially drawn and then annealed under various conditions by controlling the applied strain and annealing condition (constant strain or constant stress). When the PPN monofilament is drawn uniaxially at 50 °C, the stress–strain curve shows that the stress softening is observed at small strain and that the stress is hardened at the strain of ca. 2 due to full stretching of chain between entanglement points, as shown in Fig. 4. PPN monofilaments for obtaining the X-ray fiber diagram were prepared by drawing up to the strain between 2 and 6, followed by annealing under constant strain or constant

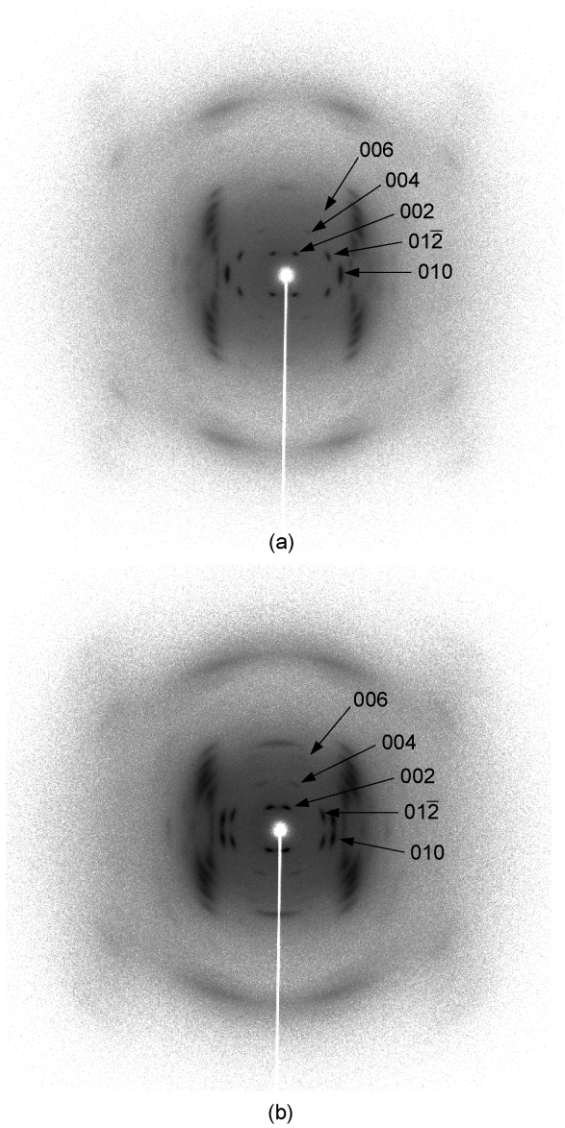

Fig. 5. X-ray fiber diagrams of PPN monofilaments after drawn to the strain of 6 and annealed at 100 °C: (a) under constant stress; (b) under constant strain.

stress condition. X-ray fiber diagrams for the samples annealed under constant strain and under constant stress condition after drawing up to the strain of 6 are represented in Fig. 5, where the index of reflections are based on the unit cell of PPN. Determination of the unit cell structure is described in Section 3.2. Comparison of two diagrams of samples annealed under constant stress and under constant strain reveals some differences for the positions of diffraction spots in Fig. 5. In order to clarify the reason for these differences, a careful inspection should be given to the possibility of crystal transformation induced by applied stress or strain. The X-ray diffractograms shown in Fig. 6 are obtained from circular integration of the intensities of the X-ray fiber diagrams of PPN monofilaments prepared under various conditions. There is no significant difference between the X-ray diffractograms except for the intensity of

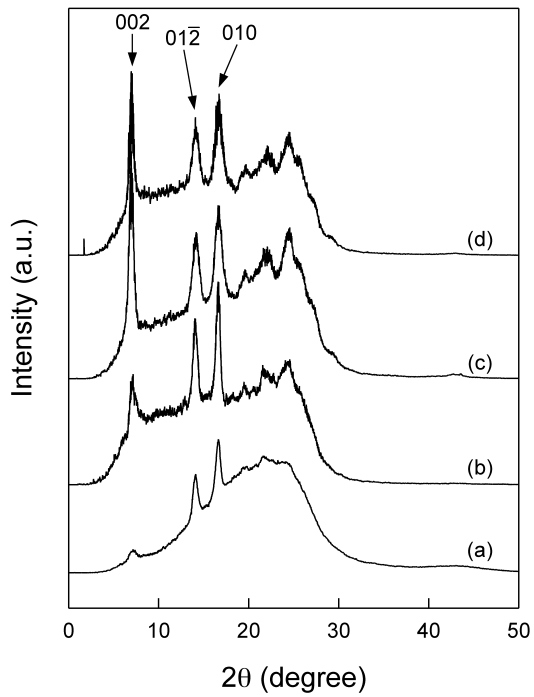

Fig. 6. X-ray fiber diffractograms of PPN monofilaments annealed at 100 °C: (a) without strain; (b) under constant strain of 2; (c) under constant stress after applying strain of 6; (d) under constant strain of 6.

002 reflection, as can be seen in Fig. 6. Since the difference of the relative intensity of 002 reflection arises from different orientation of crystals to the fiber axis, it is a natural consequence that the relative intensity of 002 reflection becomes different according to the magnitude of applied strain. Therefore, it can be thought that the difference between the X-ray fiber diagrams shown in Fig. 5 is caused by the difference in crystal orientation to the fiber axis rather than the stress-induced crystal transformation.

The degree of crystal orientation to the fiber axis can be calculated from the azimuthal scans for 010 and 002 reflections, as shown in Fig. 7. If the crystal orientation is parallel to the fiber axis, the 010 reflection should be observed at azimuthal angle (β) of 0 or 180°, corresponding to the equatorial line of fiber diagram. The deviation from the equatorial line ($\beta = 0$ or 180°) represents the crystal orientation relative to the fiber axis. From comparison between the azimuthal scans for the 010 and 002 reflections, the degree of crystal orientation for the samples annealed under constant stress and constant strain are determined to be 2.3 and 9.4°, respectively.

The chemical structure of poly(pentamethylene terephthalate) (PPT) is similar to that of PPN except a naphthalene ring in PPN replaced by a benzene ring. It has been reported that PPT has two different crystal structures depending upon the applied stress [17,18]. One form (α) is preferred at room temperature under no stress. The chains in α-form crystal do not take fully extended conformation, whereas the other form (β) induced by stress takes fully extended

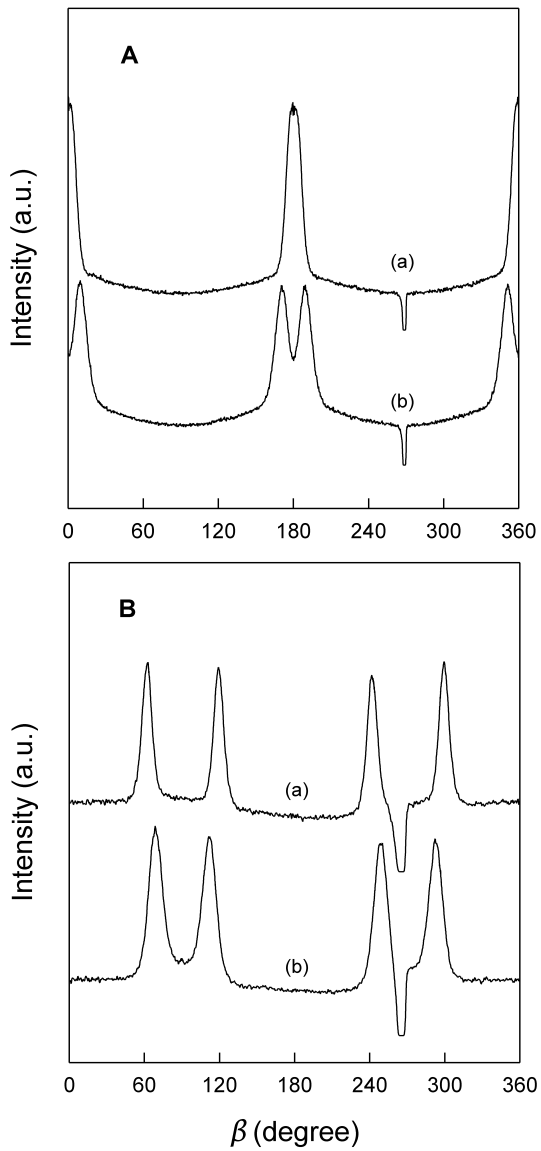

Fig. 7. Azimuthal scans of the 010 reflection (A) and 002 reflection (B) on the X-ray fiber diagrams shown in Fig. 5(a) and (b).

conformation. The α-form of PPT transforms reversibly to the β-form under the stress, whereas PPN does not exhibit the stress-induced crystal transformation.

3.2. Crystal structure analysis by X-ray diffraction

Of the most important in X-ray fiber diagram is the distance between the diffraction layers including the equatorial line, which corresponds to the crystallographic repeat length of the unit cell. In order to minimize the crystal orientation to the fiber axis and to obtain the well-layered diffraction pattern, it is required that PPN monofilament for crystal structure analysis is annealed under constant stress. However, it is not always possible to obtain the X-ray fiber diagrams having clearly defined layer lines, because of some degree of crystal orientation. As a result, extensive attempts should be given to index reflections and to determine the unit cell parameters. Considering the crystal orientation, the fiber repeat of PPN was estimated to be 2.916 nm, which is shorter than two chemical repeat length (3.420 nm) of fully extended conformation of PPN. Therefore, it is reasonable to assume that the pentamethylene sequence in the crystal is not in the fully extended conformation. Indexing of diffraction spots in the X-ray fiber diagram yielded a triclinic unit cell with a dimension of $a = 0.457$ nm, $b = 0.635$ nm, $c = 2.916$ nm, $\alpha = 121.6°$, $\beta = 90.4°$, and $\gamma = 87.6°$. The observed and calculated d-spacings are given in Table 1. The reliability parameter of indexing ($R_{\text{X-ray}}$) after refinement of unit cell dimension was 2.37%, indicating that the identification of unit cell is quite reasonable. The crystal density calculated from the unit cell parameters is 1.311 g cm^{-3}, which is close to the experimental value (1.330 g cm^{-3}) estimated using the following equation

$$\frac{1}{\rho} = \frac{x_c}{\rho_{cr}} + \frac{1 - x_c}{\rho_{am}}$$

where x_c, ρ, ρ_{cr} and ρ_{am} are the degree of crystallinity determined by X-ray measurement, the density of sample, the density of crystalline phase, and the density of amorphous phase, respectively. The density (ρ_{am}) of the amorphous sample was 1.251 g cm^{-3}.

From comparison between the measured crystal density and the calculated one, and from comparison between the crystallographic repeat length of c-axis and the chemical repeat length of fully extended conformation, it can be concluded that one polymer chain passes through an a–b plane of unit cell and that two chemical repeat units are extended in the c-axis of unit cell. Systematic absence of 00l reflection is found when l is odd number, as can be seen in X-ray fiber diagrams of Fig. 5. This suggests that two naphthaloyl residues are approximately related by a 2/1 screw axis or by centres of symmetry at the centres of the naphthalene rings. Since the midpoints of two naphthaloyl groups of PPN backbone in the triclinic unit cell become crystallographic centres of symmetry, the $P\bar{1}$ space group is assumed. Therefore, all of the bond lengths, bond angles, and torsion angles in polymer backbone should be symmetric based on these centres of symmetry.

3.3. Molecular modeling of crystal structure

The chemical repeat unit of PPN is shown in Fig. 8, where the numbering of the atoms and torsion angles are designated. In order to identify the crystal structure of PPN by molecular modeling technique, various initial molecular models of PPN satisfying the constraints such as crystallographic repeat length of c-axis, centre of symmetry and systematic absence of 00l reflections (l is odd number) were first generated in the unit cell. Then, molecular mechanics calculation was performed to minimize the total energy of the unit cell. Of all the models for crystal structure, it is found that the crystal structure with the *gauche*/*gauche*

Table 1
Comparison of calculated and observed *d*-spacings and structure factors of PPN

hkl	d_c (Å)	d_0 (Å)	$\|F_{cal,ref}\|$	$\|F_{cal}\|^a$	$\|F_{obs}\|$
010	5.403	5.367	96.11		93.06
100	4.565	4.630	17.85		21.68
110	3.567	3.527	4.50		8.72
$1\bar{1}0$	3.413		12.23		
$1\bar{2}0$	2.281		13.76		
030	1.801		25.94		
001	24.833		0.60		
101	4.504	4.559	9.41	12.39	18.55
$10\bar{1}$	4.476		8.07		
$11\bar{1}$	3.708	3.688	23.73	32.43	28.61
$1\bar{1}1$	3.550		22.11		
111	3.376	3.397	33.39	54.41	49.38
$1\bar{1}\bar{1}$	3.234		42.97		
201	2.277		19.08		
$2\bar{1}\bar{1}$	2.027		28.21		
022	12.416	12.680	2.80		3.52
$01\bar{2}$	6.310	6.349	66.29		54.97
102	4.309	4.268	25.42	32.07	38.77
$10\bar{2}$	4.261		19.56		
012	4.212	4.208	60.33		57.22
$11\bar{2}$	3.778	3.756	17.47		20.52
$1\bar{1}2$	3.625	3.632	27.85		24.23
$1\bar{1}\bar{2}$	3.034	2.982	3.07	28.18	32.86
$02\bar{2}$	2.985		27.98		
$1\bar{2}2$	2.448		21.44		
022	2.392		47.18		
033	8.278		0.36		
103	4.028	4.010	65.66	73.53	68.63
$10\bar{3}$	3.968		33.09		
$11\bar{3}$	3.761		81.73		
013	3.719	3.738	0.58	100.65	89.58
$1\bar{1}3$	3.625		58.73		
$1\bar{2}3$	2.507		32.08		
$21\bar{3}$	2.172		26.65		
044	6.208	6.245	7.53		2.03
104	3.709		70.88		
$11\bar{4}$	3.663	3.659	94.99	154.15	160.25
$10\bar{4}$	3.647		38.04		
$1\bar{1}4$	3.551		90.54		
014	3.307		10.98		
$12\bar{4}$	2.650	2.64	62.17	63.49	31.28
$1\bar{1}\bar{4}$	2.632		12.84		
$1\bar{2}4$	2.544		30.00		
024	2.106		31.61		
$2\bar{1}4$	2.105		21.94		
$03\bar{4}$	2.039		21.45		
$11\bar{5}$	3.500		67.93		
$1\bar{1}5$	3.414	3.501	81.11	108.18	99.33
105	3.391		22.44		
$10\bar{5}$	3.332		2.36		
$12\bar{5}$	2.657	2.640	54.16		25.12
$1\bar{2}5$	2.555		19.83		
$2\bar{1}5$	2.077		30.39		
$22\bar{5}$	1.890		48.40		
$01\bar{6}$	4.675		14.59		
006	4.139	4.134	50.40		10.11

Table 1 (*continued*)

hkl	d_c (Å)	d_0 (Å)	$\|F_{cal,ref}\|$	$\|F_{cal}\|^a$	$\|F_{obs}\|$
$11\bar{6}$	3.298	3.307	15.34	40.58	38.13
$1\bar{1}6$	2.236		37.57		
$02\bar{6}$	3.137		21.03		
106	3.094	3.125	32.98	59.72	64.03
$10\bar{6}$	3.040		45.13		
$12\bar{6}$	2.633		29.68		
116	2.344		22.82		
$1\bar{1}\bar{6}$	2.276		23.58		
$03\bar{6}$	2.103	2.098	11.87	12.02	6.98
$21\bar{6}$	2.067		1.86		
$2\bar{1}6$	2.036	2.019	27.85	27.98	19.23
206	2.014		2.69		
$13\bar{6}$	1.943		7.86		
$22\bar{6}$	1.881		25.57		
007	3.548		0.43		
$11\bar{7}$	3.078		26.57		
$02\bar{7}$	3.056	3.096	3.89	31.80	35.20
$1\bar{1}7$	3.036		17.03		
$10\bar{7}$	2.778		18.33		
$12\bar{7}$	2.582		20.08		
117	2.179		37.83		
$1\bar{1}\bar{7}$	2.121	2.156	38.37	53.92	48.23
$03\bar{7}$	2.114		2.07		
$21\bar{7}$	2.008	1.992	17.32	50.07	45.09
$2\bar{1}7$	1.985		46.98		
$13\bar{7}$	1.950		18.31		
207	1.935	1.947	17.57	47.12	51.01
$20\bar{7}$	1.904		39.70		
$01\bar{8}$	3.639	3.643	15.83		19.26
008	3.104	3.111	28.33		25.13
$02\bar{8}$	2.939	2.950	13.50		16.86
$11\bar{8}$	2.859	2.845	19.16	28.88	18.63
$1\bar{1}8$	2.832		21.61		
$12\bar{8}$	2.508	2.458	33.72	44.38	47.96
$1\bar{2}8$	2.436		28.84		
$03\bar{8}$	2.110	2.096	40.75		46.96
$13\bar{8}$	1.946		4.13		
$21\bar{8}$	1.942	1.935	19.26	55.52	49.21
$2\bar{1}8$	1.925		51.91		
208	1.855		25.84		
$22\bar{8}$	1.832	1.834	52.07	64.52	36.23
$20\bar{8}$	1.824		28.01		
$2\bar{2}8$	1.775		41.38		
009	2.759		0.88		
$11\bar{9}$	2.650	2.648	38.06	46.85	51.24
$1\bar{1}9$	2.634		27.33		
$12\bar{9}$	2.417		29.50		
109	2.380	2.390	5.31	50.61	
$1\bar{2}9$	2.356		39.70		
$10\bar{9}$	2.343		9.31		
$03\bar{9}$	2.091		14.26		
$1\bar{3}9$	1.874		31.24		
$2\bar{1}9$	1.861		30.68		
$22\bar{9}$	1.794	1.782	50.53	50.89	42.21
209	1.774		6.04		
$2\bar{2}9$	1.744	1.738	59.03	59.06	62.26
$20\bar{9}$	1.744		1.82		
$\bar{0}\bar{1}10$	2.908	2.921	18.30		14.89
0010	2.483		1.89		
$\bar{1}\bar{1}10$	2.456	2.459	20.05	27.43	22.32
$1\bar{1}10$	2.449		18.63		

Table 1 (*continued*)

hkl	d_c (Å)	d_0 (Å)	$\|F_{cal,ref}\|$	$\|F_{cal}\|^a$	$\|F_{obs}\|$
1010	2.198	2.185	37.69	48.52	51.25
$\bar{1}\bar{0}$10	2.166		30.56		
$\bar{1}\bar{3}$10	2.058	2.048	26.50	26.50	30.25
0110	1.909	1.913	5.77	32.19	36.13
$\bar{1}\bar{3}$10	1.903		31.67		
1310	1.851	1.842	33.63	33.63	25.88
$\bar{2}\bar{1}$10	1.799	1.786	29.64	35.54	29.35
$2\bar{1}$10	1.792		4.36		
1110	1.780		19.12		
$\bar{2}\bar{2}$10	1.750	1.722	3.90	44.83	50.30
$\bar{1}$110	1.743		16.76		
$2\bar{2}$10	1.707		20.68		
2010	1.695		35.86		
$\bar{0}\bar{2}$11	2.490		8.18		
$\bar{1}\bar{1}$11	2.281	2.276	27.12	33.07	23.58
$1\bar{1}$11	2.278		18.90		
0011	2.258		0.86		
1011	2.038	2.023	47.57	62.35	54.49
$\bar{0}\bar{3}$11	2.013		2.43		
$\bar{1}\bar{0}$11	2.010		40.23		
$\bar{1}\bar{3}$11	1.866	1.850	34.69	34.69	36.74
$\bar{2}\bar{1}$11	1.725	1.711	16.35	33.47	28.47
$2\bar{1}$11	1.723		14.51		
$\bar{2}\bar{2}$11	1.701		23.45		
1111	1.673		9.64		
$\bar{0}\bar{1}$12	2.397		12.28		
$\bar{0}\bar{2}$12	2.338		9.64		
$1\bar{1}$12	2.123	2.120	27.29	41.28	45.98
$\bar{1}\bar{1}$12	2.122		24.88		
$\bar{1}\bar{2}$12	2.097		10.44		
0012	2.069		15.20		
$1\bar{2}$12	2.065		0.47		
$\bar{0}\bar{3}$12	1.959	1.962	32.21	32.21	28.50
$\bar{1}\bar{0}$12	1.872	1.862	15.96	15.96	21.24

[a] $|F_{cal}| = (\sum |F_{cal,ref}|^2)^{1/2}$ for overlapping reflections.

conformation in the middle part of the pentamethylene units has a minimum energy, and the structure factors calculated from the energy-minimized crystal structure are comparable to experimental structure factors. The *R* factor calculated by comparing the observed structure factors ($|F_{obs}|$) with calculated ones ($|F_{cal}|$) is 17.9%. In this refinement, the overall isotropic temperature factor of 5.8 Å^2 was used. The observed structure factors of all the diffraction spots examined are compared with the calculated ones, as listed in Table 1. The bond lengths and bond angles of the final structural model are listed in Table 2, and the torsion angles with the minimum energy are determined to be $\phi_1 = -\phi_1' = -177.7°$, $\phi_2 = -\phi_2' = 179.0°$, $\phi_3 = -\phi_3' = 172.5°$, $\phi_4 = -\phi_4' = 177.3°$, $\phi_5 = -\phi_5' = 72.6°$, $\phi_6 = -\phi_6' = 75.8°$, $\phi_7 = -\phi_7' = 174.7°$, $\phi_8 = -\phi_8' = 172.7°$, $\phi_9 = -\phi_9' = 178.9°$, and $\phi_{10} = -\phi_{10}' = 170.0°$. Fractional coordinates of each atom in the unit cell are listed in Table 3. The carboxylic groups in the PPN backbone are nearly coplanar to the naphthalene ring plane, and the middle part of each pentamethylene unit consists of the *gauche*/*gauche* conformation. The molecular packing in the unit cell is shown in Fig. 9, where two naphthalene groups are in face-to-face arrangement. In this type of molecular arrangement, successive naphthaloyl groups are inclined to the crystal *c*-axis by opposite inclination, resulting in a Z-shaped arrangement. The Z-shaped arrangement of chain backbone

Table 2
Bond lengths and bond angles in the crystal of PPN

Bond length		Bond angle	
Bond	Length (Å)	Bond	Angle (°)
C1–C2	1.403	C1–C2–C3	121.3
C1–C4	1.387	C1–C4–C5	121.4
C1–C6	1.481	C1–C6–O2	112.8
C2–C3	1.378	C2–C1–C4	119.4
C3–C5′	1.417	C2–C1–C6	121.4
C4–C5	1.410	C2–C3–C4	120.0
C5–C5′	1.442	C3–C5′–C5	118.6
C6–O1	1.212	C4–C5–C5′	118.8
C6–O2	1.367	C6–O2–C7	117.8
C2–C7	1.444	O2–C7–C8	107.5
C7–C8	1.525	C7–C8–C9	116.9
C8–C9	1.531	C8–C9–C10	117.5
C9–C10	1.534	C9–C10–C11	114.2
C10–C11	1.527	C10–C11–O3	109.9
C11–O3	1.443	C11–O3–C12	117.1
C3–C2	1.369	O3–C12–C13	112.6
C12–O4	1.213	C12–C13–C14	121.2
C12–C13	1.482	C13–C14–C15	121.4
C13–C14	1.403	C13–C16–C17	121.3
C13–C16	1.387	C14–C13–C16	119.3
C14–C15	1.378	C14–C15–C17′	120.6
C15–C17′	1.417	C15–C17′–C17	118.5
C16–C17	1.410	C16–C17–C17′	118.9
C17–C17′	1.442		

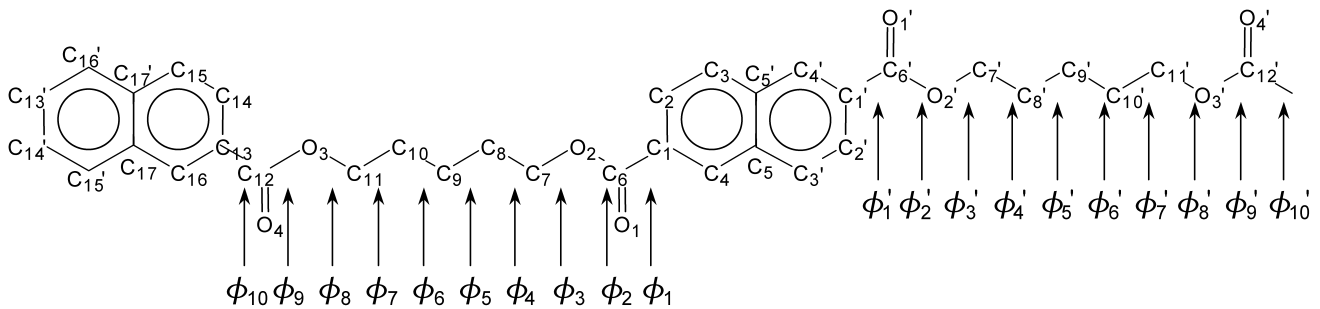

Fig. 8. Schematic representation of crystallographic repeat unit of PPN and numbering of atoms and torsion angles.

Table 3
Fractional atomic coordinates in the crystal of PPN

Atom	*x/a*	*y/b*	*z/c*
C1	0.2749	−0.0957	0.4153
C2	0.3032	0.1571	0.4529
C3	0.1783	0.2686	0.5037
C4	0.1161	−0.2359	0.4293
C5	−0.0160	−0.1299	0.4807
C6	0.4116	−0.2166	0.3608
C7	0.7171	−0.1562	0.3021
C8	0.8409	0.0611	0.3014
C9	0.0207	0.0003	0.2515
C10	0.4547	−0.0812	0.1993
C11	0.6893	0.1299	0.1981
C12	0.3803	0.1988	0.1398
C13	0.2685	0.0882	0.0844
C14	0.3886	−0.1369	0.0419
C15	0.2894	−0.2380	0.9901
C16	0.0456	0.2118	0.0740
C17	−0.0620	0.1161	0.0215
O1	0.3956	−0.4307	0.3247
O2	0.5693	−0.0582	0.3534
O3	0.5638	0.0385	0.1456
O4	0.3257	0.4061	0.1778
H2	0.4260	0.2729	0.4427
H3	0.2037	0.4669	0.5326
H4	0.0900	−0.4342	0.4004
H7[a]	0.5645	−0.2557	0.2690
H7′[a]	0.8928	−0.2918	0.2968
H8	0.9815	0.1568	0.3369
H8′	0.6573	0.1929	0.3082
H9	0.1894	−0.1438	0.2439
H9′	0.1403	0.1657	0.2613
H10	0.7014	−0.2261	0.1911
H10′	0.0142	−0.1653	0.1653
H11	0.8387	0.2783	0.2071
H11′	0.5167	0.2128	0.2294
H14	0.5719	−0.2343	0.0487
H15	0.3914	−0.4116	0.9572
H16	−0.0521	0.3890	0.1065

[a] H7 and H7′ mean hydrogens which are covalent-bonded to C7.

is generally observed in crystal structures of aromatic polyesters with odd number of methylene unit in their backbone, e.g. PTN [10], PPT α-form [18], and poly (trimethylene terephthalate) [19,20].

4. Conclusions

As a primary study of PPN, its crystal structure was identified by using X-ray fiber diffraction and molecular modeling methods. The unit cell of PPN was found to be triclinic with $a = 0.457$ nm, $b = 0.635$ nm, $c = 2.916$ nm, $\alpha = 121.6°$, $\beta = 90.4°$, and $\gamma = 87.6°$. The unit cell has one polymer chain with two chemical repeating units, and the calculated crystal density is 1.311 g cm^{-3}. The chain in unit cell possesses two crystallographic centres of symmetry (space group $P\bar{1}$). The middle part of each pentamethylene unit in PPN backbone takes *gauche*/*gauche* conformation.

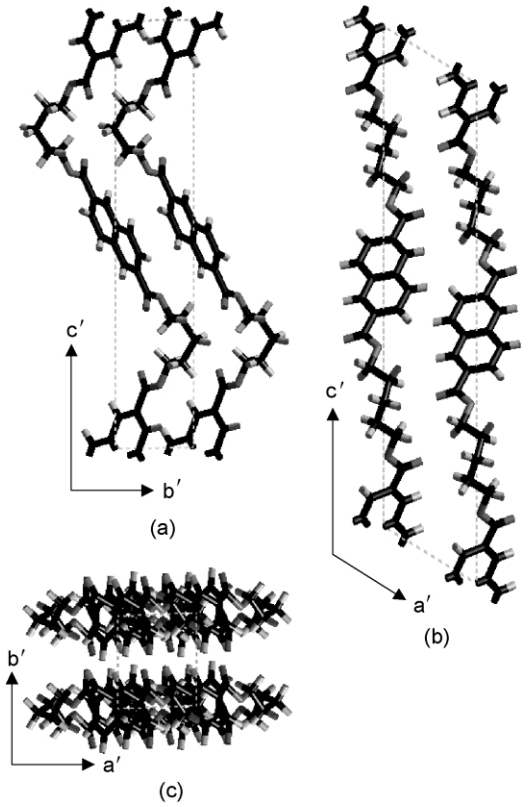

Fig. 9. Molecular packing of PPN backbone in triclinic unit cell: (a) projection along *a*-axis; (b) projection along *b*-axis; (c) projection along *c*-axis.

The packing mode is of the face-to-face arrangement of two naphthalene rings. Unlike PEN, PTN, PBN, and PHN belonging to P*m*N family, PPN does not show the crystal transformation induced by temperature and/or stress.

Acknowledgements

One of authors (S.C. Lee) thanks the Korea Science and Engineering Foundation for their financial support through the Basic Research Program (grant no.: R02-2001-01225).

References

[1] Duling IN, Chester W. US Patent, 3,436,376; 1969.
[2] Mencik Z. Chem Prum 1967;17:78.
[3] Liu J, Myers J, Geil PH, Kim JC, Cakmak M. SPE Antec Tech 1997; 43.
[4] Buchner S, Wiswe D, Zachmann HG. Polymer 1989;30:480.
[5] Watanabe H. Kobunshi Ronbunshu 1976;33:299.
[6] Koyano H, Yamamoto Y, Saito Y, Yamanobe T, Komoto T. Polymer 1998;39:4385.
[7] Yokouchi M, Sakakibara Y, Chatani Y, Tadokoro H, Tanaka T, Yada K. Macromolecules 1976;9:266.
[8] Hall IH, Pass MG. Polymer 1976;17:807.
[9] Nitzsche SA, Wang YK, Hsu SL. Macromolecules 1992;25:2397.
[10] Jeong YG, Jo WH, Lee SC. Proc Kor Text Conf 1999;32(2):307.
[11] Jeong YG, Jo WH, Lee SC. Polym J 2001;12:913.

[12] Jeong YG, Jo WH, Lee SC. Unpublished data.
[13] Sun H. J Phys Chem B 1998;102:7338.
[14] Ewald PP. Ann Phys 1921;64:253.
[15] Karasawa N, Goddard III WA. J Phys Chem 1989;93:7320.
[16] Jang SS, Jo WH. Fibers Polym 2000;1:18.
[17] Hall IH, Pass MG, Rammo NN. J Polym Sci, Part B: Polym Phys 1978;16:1409.
[18] Hall IH, Rammo NN. J Polym Sci, PartB: Polym Phys 1978;16:2189.
[19] Dandurand SP, Perez S, Revol JF, Brisse F. Polymer 1979;20:419.
[20] Desborough IJ, Hall IH, Neisser JZ. Polymer 1979;20:545.